Open Access Full Text Article

ORIGINAL RESEARCH

The effects and mechanisms of a biosynthetic ginsenoside 3β,12β-Di-O-Glc-PPD on non-small cell lung cancer

Lu-Lu Huang[1,2]
Mei Tang[1,2]
Qian-Qian Du[1,2]
Chun-Xia Liu[1,2]
Chen Yan[2]
Jin-Ling Yang[3]
Yan Li[1,2]

[1]Department of Pharmacology, Beijing Key Laboratory of New Drug Mechanisms and Pharmacological Evaluation Study, Institute of Materia Medica, Chinese Academy of Medical Sciences and Peking Union Medical College, Beijing 100050, People's Republic of China; [2]Department of Pharmacology, Institute of Materia Medica, Chinese Academy of Medical Sciences and Peking Union Medical College, Beijing 100050, People's Republic of China; [3]Department of Biosynthesis, State Key Laboratory of Bioactive Substance and Function of Natural Medicines and Key Laboratory of Biosynthesis of Natural Products of National Health and Family Planning Commission, Chinese Academy of Medical Sciences and Peking Union Medical College, Beijing, 100050, People's Republic of China

Correspondence: Yan Li
Institute of Materia Medica, Chinese Academy of Medical Sciences and Peking Union Medical College, 1 Xian Nong Tan Street, Beijing 100050, People's Republic of China
Tel +86 10 6316 9181
Email lyhzytt@163.com

Background: A biosynthetic ginsenoside, 3-O-β-D-glucopyranosyl-12-O-β-D-glucopyrano-syl-dammar-24-ene-3β, 12β, 20S-triol ($C_3C_{12}PPD$), showed antitumor activity against many tumor cells in vitro, especially had better anti-lung cancer activity than Rg3 in vitro and in vivo. However, the effects and molecular mechanisms of $C_3C_{12}PPD$ on non-small cell lung cancer (NSCLC) remain unclear. According to previous studies, we hypothesized ginseno-side $C_3C_{12}PPD$ could inhibit the tumor growth of NSCLC by targeting proliferation, migration and angiogenesis.

Methods: A thiazolyl blue tetrazolium bromide assay (MTT) was performed to evaluate cell viability. Additionally, Transwell and tube formation assays were conducted to analyze cell migration and angiogenesis. The Lewis and A549 tumor xenograft experiments were also performed to investigate the effects of $C_3C_{12}PPD$ on tumor growth in vivo, Western blotting and IHC assay were performed to analyze protein expression.

Results: $C_3C_{12}PPD$ could effectively inhibit the proliferation and migration of lung cancer cells, and tube formation of EA.hy926 cell. Ginsenoside $C_3C_{12}PPD$ suppressed Lewis and A549 tumor growth in vivo without obvious side effects on body weight and the hematology index. In addition, the Western blot analysis revealed that the effects of $C_3C_{12}PPD$ on lung cancer were mediated by inhibiting Raf/MEK/ERK, AKT/mTOR and AKT/GSK-3β/β-Catenin signaling pathways. Finally, $C_3C_{12}PPD$ could significantly inhibit the proliferation index and vessel number in Lewis xenograft tumors analyzed by IHC.

Conclusion: The results of the present study suggest that ginsenoside $C_3C_{12}PPD$ may serve as a potential therapeutic candidate compound against NSCLC.

Keywords: $C_3C_{12}PPD$, NSCLC, Raf/MEK/ERK, AKT/mTOR, AKT/GSK-3β/β-Catenin

Introduction

Lung cancer remains the leading cause of cancer incidence and mortality world-wide, with 2.1 million new lung cancer cases and 1.8 million deaths predicted in 2018, representing close to 1 in 5 (18.4%) global cancer deaths, and about 80% of all lung cancer cases presenting as NSCLC.[1,2] Despite of recent advances in the treatment for NSCLC, the prognosis and survival time remain unsatisfactory, there are growing requirements for innovative therapeutic strategies to decrease the mortality of NSCLC.[3]

The use of Panax ginseng in traditional Chinese medicine dates back to about 5000 years ago, and pharmacopeia across Japan, Korea, USA, Canada, Germany, UK, France and Austria recognize its vitality-restoration ability.[4,5] In recent years,

global research on P. ginseng has increased rapidly. Ginsenosides, isolated from ginseng, have various beneficial properties, including anti-cancer, neuroprotection, cardioprotectiion, boosting immunity.[5–7] Among them, ginsenoside Rg3, protopanaxadiol (PPD)-type ginsenoside, has been developed as a novel drug for cancer.[8,9] Researchers have done a lot of work in modifying the structure of ginsenoside Rg3 to improve biological activity, bioavailability, and alleviate toxicity.

$C_3C_{12}PPD$, one of novel ginsenosides, has the same molecular weight and number of sugar moiety as Rg3, was produced by chemical semi-synthesis about 20 years ago, and could been produced in large-scale by microbial fermentation since 2017. Previous studies proved that ginsenoside $C_3C_{12}PPD$ exhibited remarkable activity against diverse human cancer cell lines and a higher anti-lung cancer activity than Rg3.[10–12] However, further effects and mechanisms of $C_3C_{12}PPD$ on NSCLC are scarely reported. According to the studies of ginsenosides,[13,14] we hypothesized $C_3C_{12}PPD$ could inhibit the proliferation, migration and angiogenesis of NSCLC mediated by Raf/MEK/ERK, AKT/mTOR and AKT/GSK-3β/β-Catenin signaling pathways.

Ginsenosides exhibited excellent anticancer activity in p53-wildtype cell lines, so we chose p53-wildtype NSCLC cell lines LLC and A549 in this study.[9,15–17] We evaluated the effects of $C_3C_{12}PPD$ on NSCLC in vitro and in vivo, explored its possible mechanisms, and hope to provide an experimental basis for its further study.

Materials and methods
Cell culture
Human umbilical vein endothelial cell lines EA.hy926, human lung cancer cell lines NCI-H1650, NCI-H1975, NCI-H460 and A549 and murine lung cancer cell lines LLC were purchased from the cell center of the Chinese Academy of Medical Sciences and Pecking Union Medical College (Beijing, China). The EA.hy926, NCI-H1975 and LLC cells were cultured in Dulbecco's modified Eagle's medium (DMEM, Invitrogen; Thermo Fisher Scientific, Inc., Waltham, MA, USA), the NCI-H1650, NCI-H460 and A549 cells were cultured in RPMI-1640 (Invitrogen; Thermo Fisher Scientific, Inc.). All cell cultures were supplemented with 10% fetal bovine serum (FBS; YHSM, Beijing, China), 100 IU/mL penicillin and 100 μg/mL streptomycin. All cell lines were incubated at 37°C with 5% CO_2.

Drugs and compounds
The $C_3C_{12}PPD$ was provided by Institute of Materia Medica, Chinese Academy of Medical Sciences and Peking Union Medical College (HPLC purity >98%). Taxol was obtained from the Beijing Union Pharmaceutical Factory (Beijing, China). According to the reference, $C_3C_{12}PPD$ was dissolved in dimethyl sulfoxide (DMSO) in vitro experiments, and was dissolved in a solution of 25% PEG400 in vivo experiments.[10] For the in vivo experiments, Taxol was diluted by 0.9% NaCl prior to use.

MTT assay
NCI-H1650, NCI-H1975, NCI-H460, A549 and LLC cell lines were seeded in a 96-well plate. After incubation for 24 h, the cells were treated with varied concentrations (4.0 μmol/L, 20.0 μmol/L, 100.0 μmol/L and 500.0 μmol/L) of $C_3C_{12}PPD$ or DMSO as vehicle. After incubation for 120 h, a total of 50 μL MTT stock solutions (2 mg/mL, Solarbio, Beijing, China) was added to each well. The 96-well plates were subsequently incubated for a further 4 h at 37°C. The medium was replaced with DMSO (Biosharp, Inc., Hefei, China; 150 μL/well), following gentle agitation, an ELISA reader (Bio-Rad Laboratories, Hercules, CA, USA) was used to measure the absorbance at 570 nm. Three parallel samples were measured in each cell line. The absorbance values were normalized to the values obtained for vehicle-treated cells to determine the percentage of surviving cells. The median inhibitory concentration (IC_{50}) was assessed from the dose response curve.[10] The experiment was repeated three times.

Cell migration assay
The cell migration assay was performed using Transwell inserts containing polycarbonate filters with 8.0-μm pores. Cells ($1×10^6$ cells/well) were suspended in 200 μL 0.1% bovine serum albumin (BSA, Solarbio, Beijing, China) with or without the different concentrations of $C_3C_{12}PPD$, and were seeded into the upper chamber; a total of 600 μL normal medium with 10% FBS was placed in the lower chambers. After 18 h incubation in 5% CO_2 at 37°C, the cells on the underside of the chamber were fixed with methanol, and stained with hematoxylin and eosin (H&E) and photographed in 4 randomly-selected fields (×400 magnification, Olympus IX70, Olympus Corporation, Tokyo, Japan). The number of migrated cells in the 4 randomly-selected fields of each membrane were counted, and 3 parallel samples for each cell line were measured.

Tube formation assay

A total of 5,000 EA.hy926 cells, that had been treated or untreated with $C_3C_{12}PPD$ were seeded into a 96-well plate pre-coated with Matrigel. Following incubation at 37°C for 5 h, the EA.hy926 cells were examined for capillary-like tube formation and photographed under a microscope (×100 magnification, Olympus IX70, Olympus Corporation). Three parallel samples for each concentration were run.

Tumor implantation in lewis and A549 xenograft models

All animal studies were in compliance with policies of the Institute of Material Medical Animal Care and Use Committee. All animal protocols conformed to the Guidelines for the Care and Use of Laboratory Animals, and the study protocol was approved by the Animal Care and Use Committee of Chinese Academy of Medical Sciences and Peking Union Medical College.

Lewis lung cancer xenograft model

C57BL/6 mice (males, 16–18 g) were purchased from BEIJING HFK BIOSCIENCE CO., LTD (Beijing, China). LLC cells were harvested and washed 3 times with normal saline. The cells were counted and diluted to $5×10^7$ cells/mL. The C57BL/6 mice were subcutaneously implanted with 0.2 mL of the cell suspension in their left flank. After 24 h inoculation, the C57BL/6 mice were randomly divided into 3 groups, 5 animals in each group. One group received gavage (p.o.) of 25% PEG400 as a model control. Another group received an intraperitoneal injection of 15.0 mg/kg Taxol (twice a week), and another group received p.o. of 10.0 mg/kg of $C_3C_{12}PPD$ for 10 days. When the tumor volume of control group was about 2000 mm^3, the mice were euthanized and tumors were excised, weighed and photographed. The inhibition rate (IR) of tumor growth was calculated using the following formula: IR (%) = [(A − B)/A]/100, where A is the average tumor weight of model control, B is the average tumor weight of treatment groups. The tumor tissues were stored at –80°C for subsequent analyses.

A549 human lung cancer xenograft model

BALB/c/nu nude mice (males, 15–19 g) were purchased from IFDC Institute for Laboratory Animal Resources (Beijing, China). A549 cells ($1×10^7$) were subcutaneously implanted in the left flank of each mouse.

When tumors grew to ~200 mm^3, tumor-bearing mice were randomly separated into three groups, 5 animals in each group. One group received p.o. of 25% PEG400 as a model control group, another group received an intraperitoneal injection of 25.0 mg/kg Taxol (twice a week), and the remaining group received p.o. of 10.0 mg/kg of $C_3C_{12}PPD$ for 10 days. Tumor size was measured with vernier calipers twice a week. When the tumor volume of control group was about 1500 mm^3, the mice were euthanized, and the tumors were excised, weighed and photographed.[18] Tumor volume = width × width × length/2, Relative tumor volume (RTV) = V_t/V_0 (V_t: the measured tumor volume every time, V_0: the starting volume). The tumor tissues were stored at –80°C for subsequent analyses.

Western blot analysis

Pooled tissues from 3 randomly-selected tumors from the Lewis xenograft mice of the control, 15.0 mg/kg Taxol and 10.0 mg/kg $C_3C_{12}PPD$ groups; and the A549 xenograft mice of the control, 25.0 mg/kg Taxol and 10.0 mg/kg $C_3C_{12}PPD$ groups; LLC and A549 cells that had been treated with various concentrations of $C_3C_{12}PPD$ for 72 h, were lysed using RIPA buffer for 40 mins on ice. Subsequently, the cell lysates from the aforementioned groups were centrifuged at 12,000 rpm for 30 mins at 4°C. Nuclear lysates were prepared according to the protocol of Nuclear and Cytoplasmic Extraction kit (Beijing ComWin Biotech Co., Ltd., Beijing, China). The concentrations of proteins were determined by BCA assay. A total of 40 µg proteins were loaded per lane, and then separated on SDS-PAGE and then transferred onto a 0.4 µm nitrocellulose membrane (Bio-Rad Laboratories, Inc.). The membranes were blocked with 5% skimmed milk in TBST for 2 h at 25°C, and were then incubated overnight at 4°C with the primary antibodies (VEGF antibody, Abcam; the remaining antibodies were purchased from Cell Signaling Technology, Inc., Danvers, MA USA). Following washing three times with Tris-buffered saline containing 1% Tween®-20 (Beijing Solarbio Science & Technology Co., Ltd.), the membranes were incubated with horseradish peroxidase-conjugated anti-rabbit or anti-mouse IgG (Santa Cruz Biotechnology, Inc.), and measured using an ECL Western blot detection and analysis system (Applygen Technologies Inc., Beijing, China). β-actin was used as a loading control for membrane proteins and nuclears were examined for equal loading by probing for Histone H3.

Immunohistochemistry

Immunohistochemical staining was performed using 4.0-μm formalin-fixed, paraffin embedded tissue sections. Antigen retrieval was carried out in citrate buffer (10 mmol/L, pH 6.0) for 15 mins at 100°C in a microwave oven. Endogenous peroxidase activity was blocked with 3% hydrogen peroxide in water for 30 mins. The tissue sections were then washed in 1×PBS and pre-blocked with fetal bovine serum for 30 mins. The slides were incubated with a primary rabbit anti-PCNA (ab18197, Abcam, Cambridge, UK), rabbit anti-CD34 (ab81289, Abcam) overnight at 4°C. The sections were then incubated with biotinylated secondary anti-rabbit IgG (Beijing Solarbio Science & Technology Co., Ltd., Beijing, China) for 1 h. Following washing with 1×PBS, tissue sections were incubated with Vectastain ABC reagent (Santa Cruz Biotechnology, Inc., Dallas, TX, USA). The immune complex was visualized using DAB substrate solution (Santa Cruz Biotechnology, Inc.). Each section was examined under a magnification of ×200, and analyzed with ImageJ Launcher (National Institutes of Health, Bethesda, MD, USA).[19]

Statistical analysis

Data are expressed as the mean ± the standard deviation. Statistical analysis to examine the differences between two groups was performed using a unpaired Student's t-test and to examine the differences among multiple groups was performed using a One-Way ANOVA and Dunnett's post hoc test. $P<0.05$ was considered to indicate a statistically significant difference. Statistical analyses were performed using Microsoft Excel 2016.0 (Microsoft Corporation, Redmond, WA, USA) and GraphPad Prism 5.01 (La Jolla, CA, USA).

Results

C₃C₁₂PPD inhibited the proliferation of lung cancer cells

The growth inhibitory effect of $C_3C_{12}PPD$ was evaluated in a panel of 5 lung cancer cell lines using MTT assay. An inhibition in cell viability was observed following treatment with $C_3C_{12}PPD$ for 120 h, with IC_{50} values ranging between 60 μmol/L and 260 μmol/L (Table 1).

C₃C₁₂PPD inhibited migration of LLC and A549 cells

The Transwell assay was performed to evaluate the effect of $C_3C_{12}PPD$ on the migration capacity of LLC and A549 NSCLC cells. As presented in Figure 1A and B, $C_3C_{12}PPD$ could inhibit cell migration in a concentration-dependent manner. The inhibition rates were 37.4% and 71.1% in 100.0 μmol/L and 200.0 μmol/L $C_3C_{12}PPD$-treated LLC mouse NSCLC cells, respectively (Figure 1A). In addition, cell migration was decreased by 34.6% and 42.9% following treatment with 50.0 and 100.0 μmol/L $C_3C_{12}PPD$ respectively, in A549 human NSCLC cells (Figure 1B). The proliferation of LLC and A549 cells were not significantly influenced under the aforementioned $C_3C_{12}PPD$ concentrations, as the inhibitory rates were under 20% at 24 h for LLC and A549 cells. Taken together, these data suggested that $C_3C_{12}PPD$ could reduce the migration ability of LLC and A549 cells.

C₃C₁₂PPD inhibited the tube formation of EA.hy926 cells

The presence of blood vessels is associated with the malignancy and aggressiveness of lung cancer.[19] Therefore, an EA.hy926 cell tube formation assay was used to examine the effect of $C_3C_{12}PPD$ on angiogenesis. As illustrated in Figure 2, with administrated 100.0 μmol/L and 200.0 μmol/L $C_3C_{12}PPD$ for 5 h, the tube length was markedly decreased by 77.5% ($P<0.001$) and 88.2% ($P<0.001$) respectively. Furthermore, the proliferation of EA.hy926 cells was not influenced under the aforementioned concentrations, the proliferation inhibitory rate was 16.0±4.2% at 24 h for EA.hy926 cells. This data demonstrated that $C_3C_{12}PPD$ could significantly inhibit tube formation of EA.hy926 cells.

Table 1 The effect of $C_3C_{12}PPD$ on the proliferation of lung cancer cells

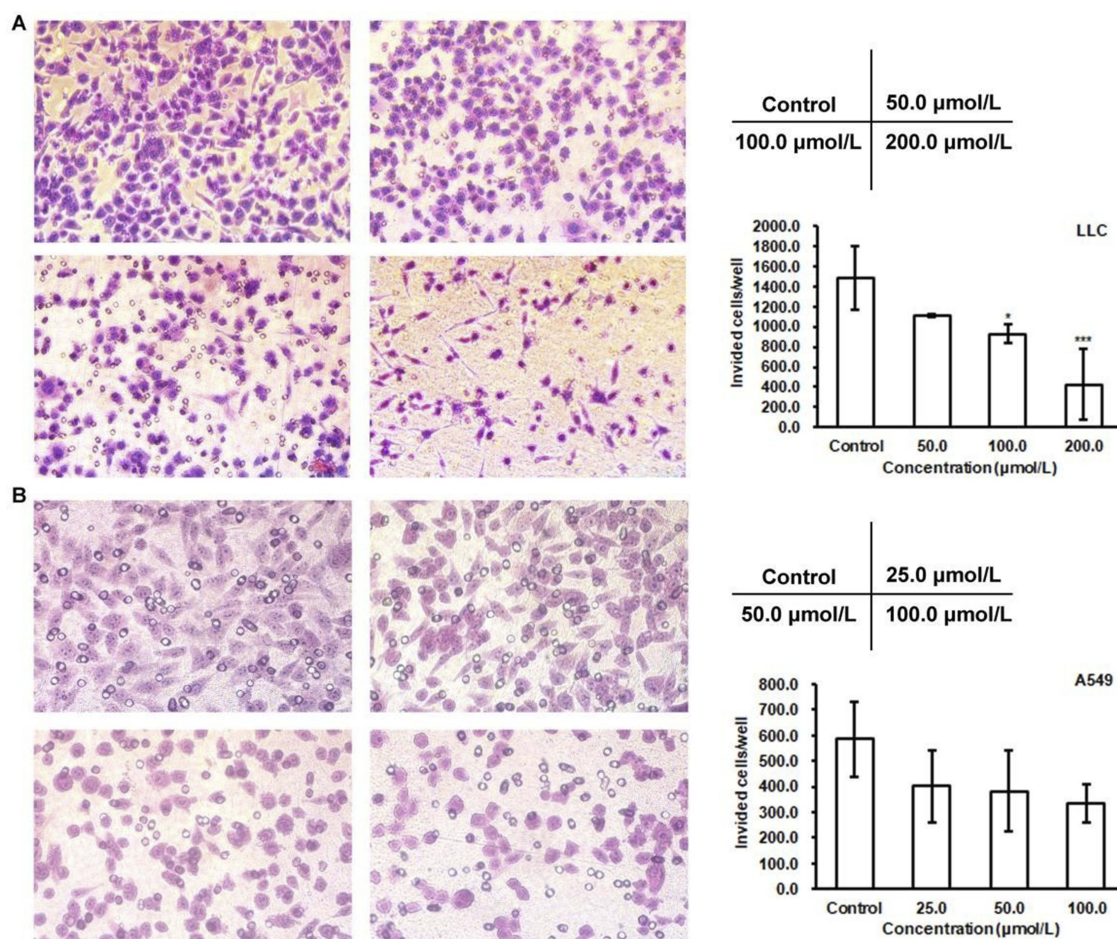|	IC₅₀ (μmol/L)				
	NCI-H1650	NCI-H1975	NCI-H460	A549	LLC
C₃C₁₂PPD	260.3±7.37	60.09±16.71	183.4±16.28	167.1±20.40	224.5±50.41

Figure 1 Effects of $C_3C_{12}PPD$ on the migration of LLC and A549 cells. Migration abilities of LLC and A549 cells were measured after treatment with different concentrations of $C_3C_{12}PPD$. Equal numbers of LLC (**A**) and A549 (**B**) cells were seeded into the upper compartment of a Transwell and allowed to transfer through polycarbonate filters for 18 h. The migrated cells were fixed and counted. The cells treated with $C_3C_{12}PPD$ exhibited a decrease in migration compared with control cells. Each sample was done in triplicate. Error bars represent the standard deviation. *$P<0.05$, ***$P<0.001$ vs Control cells.
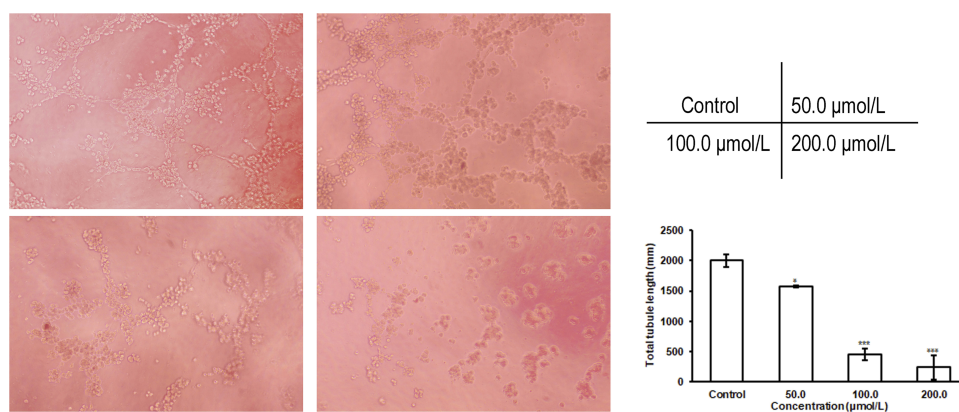

Figure 2 Effect of $C_3C_{12}PPD$ on the tube formation of EA.hy926 cells. The tube formation of EA.hy926 cells was inhibited following the treatment of $C_3C_{12}PPD$ for 5 h. Error bars represent the standard deviation. *$P<0.05$, ***$P<0.001$ vs Control cells.

Inhibitory effects of C₃C₁₂PPD on lewis and A549 lung cancer xenograft tumors in mice

In Lewis xenografts, tumor growth was suppressed in mice administrated 10.0 mg/kg $C_3C_{12}PPD$, with the tumor inhibition rate at 51.7% according to the tumor weight (Table 2, Figure 3A$_1$). In A549 xenografts, the tumor inhibition rate was 33.6% with 10.0 mg/kg $C_3C_{12}PPD$ according to the tumor weight, while the T/C (Treatment/Control) volume ratio was 60.1% (Table 3, Figure 3B$_1$ and B$_2$), suggesting that $C_3C_{12}PPD$ may inhibit the tumor growth in Lewis and A549 NSCLC xenograft models.

During the course of treatment, weight loss (Figure 3A$_2$ and B$_3$), signs of discomfort and mortality were not observed in the $C_3C_{12}PPD$ treatment groups. In Lewis and A549 xenograft models, 10.0 mg/kg $C_3C_{12}PPD$ did not cause significant decreases in typical hematological indexes, such as white blood cells (WBC), red blood cells (RBC), hemoglobin (HGB), and significantly increased RBC and HGB in Lewis xenograft model (Tables 4 and 5). These

results indicated that 10.0 mg/kg $C_3C_{12}PPD$ could inhibit tumor growth without obvious toxicity in mice.

$C_3C_{12}PPD$ influenced Raf/MEK/ERK, AKT/mTOR and AKT/GSK-3β/β-catenin signaling pathways activity

The Raf/MEK/ERK, AKT/mTOR and AKT/GSK-3β/β-Catenin signaling pathways control key cellular responses, such as cell growth, proliferation, angiogenesis and migration.[20–22] Therefore, the present study detected the expression of proteins associated with these pathways in LLC and A549 NSCLC cells and tumors treated with $C_3C_{12}PPD$.

After LLC and A549 cells were treated with $C_3C_{12}PPD$ for 72 h at 100.0 μmol/L, $C_3C_{12}PPD$ could effectively inhibit the phosphorylation c-Raf and its downstream proteins p-MEK, p-ERK and p-AKT (Figure 4A). Since mTOR is one of the targets of AKT, the p-mTOR and its downstream proteins HIF-1α, VEGF were also detected,[23,24] and it was observed that they

Table 2 The effect of $C_3C_{12}PPD$ on the tumor growth in Lewis mouse NSCLC xenograft model

Groups	Dose mg/kg	Animals (n)	Body Weight (g)		Tumor weight (g)	Inhibition (%)
		Begin/End	Begin	End		
Control		5/5	18.4±0.7	21.2±1.4	2.18±0.58	
Taxol	15.0	5/5	18.9±0.7	19.4±1.7	1.21±0.22*	44.5
C₃C₁₂PPD	10.0	5/5	18.6±1.0	21.3±0.9	1.05±0.53**	51.7

Notes: *$P<0.05$, **$P<0.01$ vs Control.
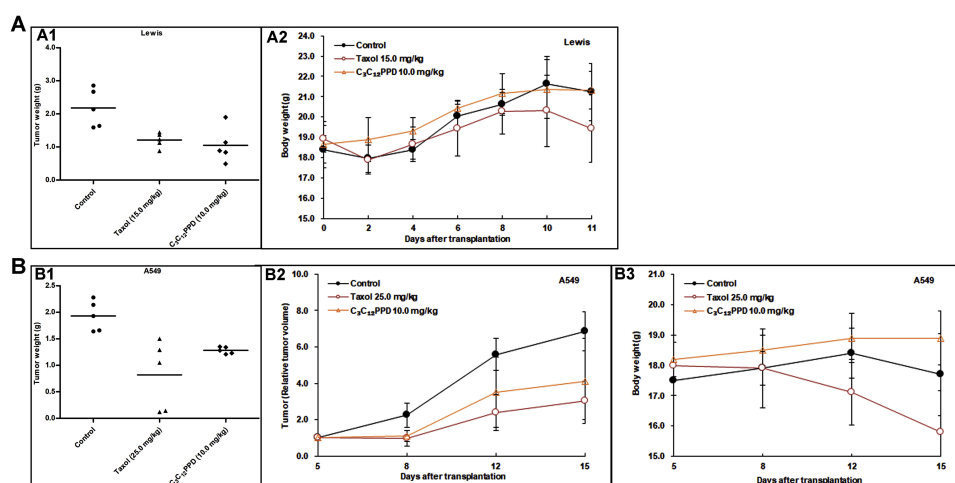

Figure 3 The effects of $C_3C_{12}PPD$ on growth of Lewis and A549 NSCLC xenografts. Activity of $C_3C_{12}PPD$ was determined in Lewis mouse NSCLC xenografts in C57BL/6 mice and in A549 human NSCLC xenografts in BALB/c/nu nude mice. Animals were randomly divided into three groups. The dosage of $C_3C_{12}PPD$ was 10.0 mg/kg. There were 5 independent tumor-bearing mice in each group. (**A**) The corresponding tumor weight (A1) and the mean body weight ± SD at different time-points (A2) for Lewis xenografts. (**B**) The corresponding tumor weight (B1), The mean volume and mean RTV (relative tumor volume = Vt/V₀) ± SD (B2) and the mean body weight ± SD at different time-points (B3) for A549 xenografts.

Table 3 The effect of $C_3C_{12}PPD$ on the tumor growth of A549 human NSCLC in athymic mouse

Groups	Dose mg/kg	Animal (n) Begin/End	Tumor volume $\bar{x} \pm SD$ (mm^3) Begin	End	Inhibition (%)	RTV $\bar{x} \pm SD$	T/C (%)	Tumor Weight $\bar{x} \pm SD$ (g)	Inhibition (%)
Control		5/5	185.1±29.3	1259.0±226.7		6.86±1.06		1.93±0.28	
Taxol	25.0	5/5	200.8±50.8	534.4±380.5**	57.6	3.05±2.34**	55.5	0.82±0.65**	57.5
$C_3C_{12}PPD$	10.0	5/5	196.1±25.6	791.4±132.8*	37.1	4.12±1.04*	60.1	1.28±0.06	33.6

Notes: *$P<0.05$, **$P<0.01$ vs Control.
Abbreviations: T/C (%), T_{RTV}/C_{RTV} ×100.0; RTV, relative tumor volume.

Table 4 The effects of $C_3C_{12}PPD$ on the peripheral blood cell count in Lewis mouse NSCLC xenograft model

Groups	Dose mg/kg	Peripheral blood count WBC (×10^9/L)	RBC (×10^{12}/L)	HGB (g/L)
Control		16.72±3.34	3.28±0.42	58.60±8.17
Taxol	15.0	4.88±2.07**	4.11±1.56	63.40±25.22
$C_3C_{12}PPD$	10.0	18.14±8.92	5.58±1.87*	87.00±23.69

Notes: *$P<0.05$, **$P<0.01$ vs Control.
Abbreviations: WBC, white blood cells; RBC, red blood cells; HGB, hemoglobin.

Table 5 The effects of $C_3C_{12}PPD$ on the peripheral blood cell count in A549 human NSCLC xenograft model

Groups	Dose mg/kg	Peripheral blood count WBC (×10^9/L)	RBC (×10^{12}/L)	HGB (g/L)
Control		15.78±12.87	5.01±0.98	102.2±17.01
Taxol	25.0	4.16±1.34	5.72±2.55	106.2±47.54
$C_3C_{12}PPD$	10.0	15.32±7.55	5.83±0.71	120.6±11.59

Abbreviations: WBC, white blood cells; RBC, red blood cells; HGB, hemoglobin.

were downregulated by 100.0 µmol/L $C_3C_{12}PPD$ (Figure 4B). At the concentration of 100.0 µmol/L $C_3C_{12}PPD$, the levels of total protein c-Raf, AKT, mTOR were also inhibited, except total protein of MEK in A549 cells remained stable (Figure 4A and 4B).

The inactivation of p-AKT also led to the decrease of p-GSK-3β and β-Catenin in LLC and A549 cells treated with 50.0 µmol/L or 100.0 µmol/L $C_3C_{12}PPD$ for 72 h. The c-MYC, LEF1 and MMP2, downstream proteins of β-Catenin, were also markedly reduced. The level of GSK-3β in LLC NSCLC cells was significantly inhibited, whereas the reduction was not obvious in A549 NSCLC cells (Figure 4C).

$C_3C_{12}PPD$ could not only inhibit Raf/MEK/ERK, AKT/mTOR and AKT/GSK-3β/β-Catenin signaling pathways in NSCLC cells, but also in tumor tissues. In Lewis and A549 xenograft tumors administrated with 10.0 mg/kg $C_3C_{12}PPD$, the levels of p-c-Raf and downstream proteins p-MEK, p-ERK and p-AKT were significantly lower than control. However, the level of total proteins did not exhibit much difference between the $C_3C_{12}PPD$-treated and control groups, except ERK of A549 xenograft tumors was significantly reduced (Figure 5A).

The expression of p-mTOR, mTOR, HIF-1α, and VEGF were significantly reduced in 10.0 mg/kg $C_3C_{12}PPD$ group compared with control (Figure 5B). In addition, in the Lewis and A549 xenograft tumors, p-GSK-3β, β-Catenin, LEF1, c-MYC and MMP2 were downregulated following administrated with 10.0 mg/kg $C_3C_{12}PPD$. The level of GSK-3β did not obviously decreased (Figure 5C). Taken together, these results indicate that the antitumor efficacy of $C_3C_{12}PPD$ may be associated with the inhibition of the Raf/MEK/ERK, AKT/mTOR and AKT/GSK-3β/β-Catenin signaling pathways.

$C_3C_{12}PPD$ inhibited PCNA and CD34 expression in lewis xenograft model analyzed by immunohistochemistry

Immunohistochemical assay was conducted to identify the alteration of PCNA and CD34 in the Lewis tumor tissues. PCNA is a marker for proliferating cells and CD34 is a vascular endothelial cell biomarker in tumor sections.[25] The IHC results presented with strong PCNA and CD34 staining in the control group, whereas the $C_3C_{12}PPD$ group exhibited weak PCNA and CD34 staining in Lewis xenograft model (Figure 6). The proliferation indexes were 20.6±1.4%, and 8.5±1.9% respectively in the control and $C_3C_{12}PPD$-treated groups. The MVD (total vessel number in four fields)
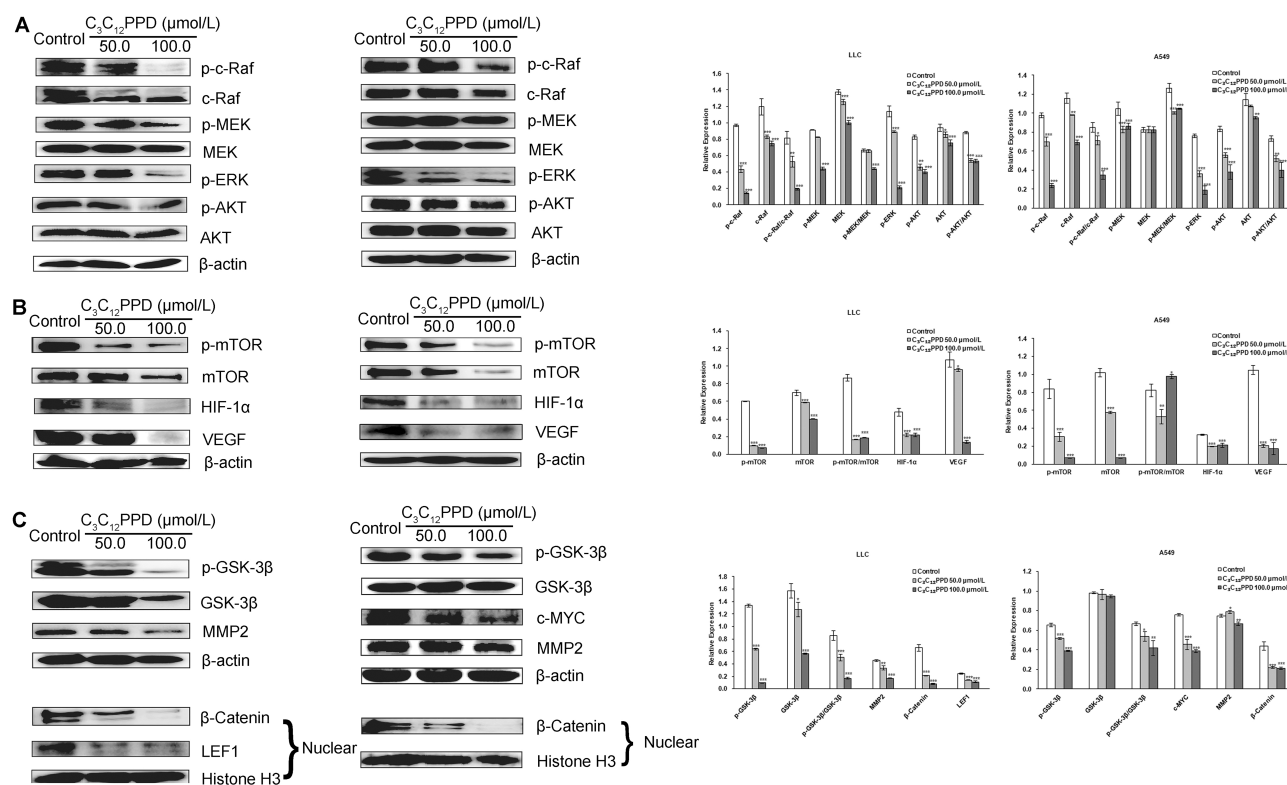
Figure 4 The effects of C₃C₁₂PPD on biomarkers related to Raf/MEK/ERK (**A**), AKT/mTOR (**B**), and AKT/GSK-3β/β-Catenin (**C**) pathways in LLC and A549 NSCLC cells. LLC and A549 cells following treatment with indicated concentrations of C₃C₁₂PPD for 72 h, and were performed with different antibodies. Each Western blotting was done at least twice. β-actin and Histone H3 were used as loading control. *$P<0.05$, **$P<0.01$, ***$P<0.001$ vs Control.
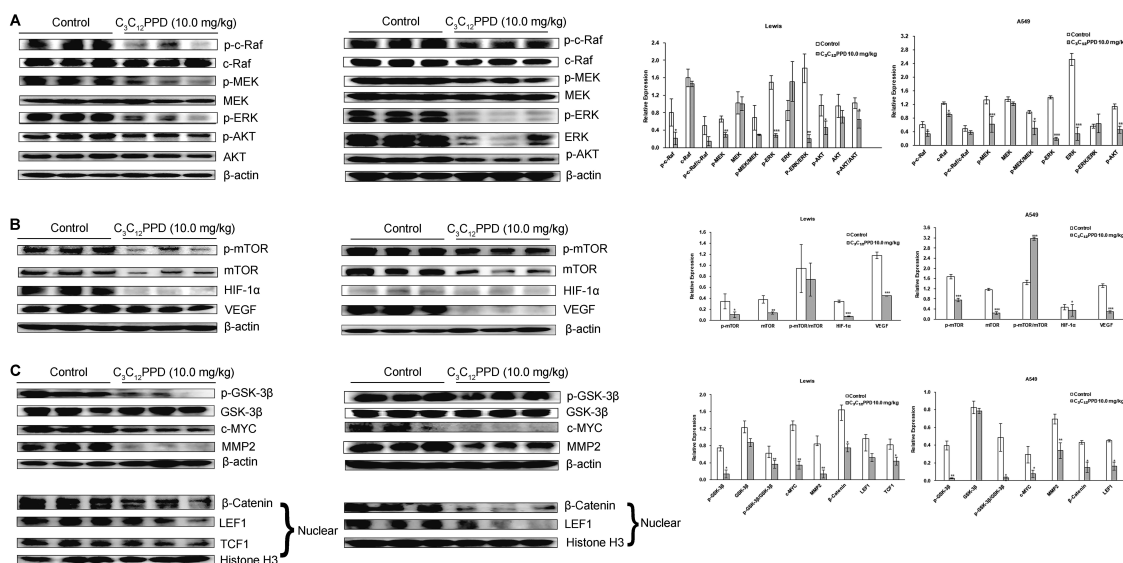

Figure 5 The effects of C₃C₁₂PPD on biomarkers related to Raf/MEK/ERK (**A**), AKT/mTOR (**B**), and AKT/GSK-3β/β-Catenin (**C**) pathways in Lewis and A549 xenograft tumors. Three lysates from one group were pooled. In this Western blot assay, each lane represented one protein pool and there were three pools each group. β-actin and Histone H3 were used as loading control. Blots were incubated with different antibodies. Representative blots were shown. Experiments were repeated at least twice. *$P<0.05$, **$P<0.01$, ***$P<0.001$ vs Control.

were 13.7±5.4% and 4.7±0.3% respectively in the control and C₃C₁₂PPD groups. These results indicated that

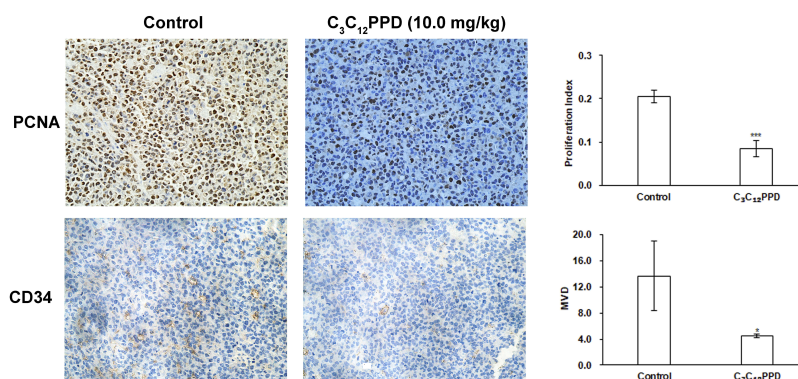C₃C₁₂PPD was effective at inhibiting tumor proliferation and angiogenesis.

Figure 6 Detection of PCNA and CD34 expression in Lewis tumor xenograft tissues analyzed by immunohistochemistry. $C_3C_{12}PPD$ inhibited Lewis tumor proliferation evaluated by PCNA staining. Decreased MVD was found in $C_3C_{12}PPD$-treated Lewis tumor tissues evaluated by CD34 staining. *$P<0.05$, ***$P<0.001$ vs Control.

Discussion

$C_3C_{12}PPD$, a ginsenoside which can be produced in large-scale by biosynthesis, has better anti-lung cancer activity than Rg3, and is a promising candidate for anti-lung cancer drug discovery.[10,11] However, the reports of the mechanisms of $C_3C_{12}PPD$ against NSCLC are rarely, which may limit its drug development. In the present study, we examined the effects of $C_3C_{12}PPD$ on mouse NSCLC cell line LLC and human NSCLC cell line A549 in vitro and in vivo, and explored it's underlying mechanisms to make an experimental basis for its drug properties.

The results demonstrated that $C_3C_{12}PPD$ could inhibit proliferation and migration in LLC mouse and A549 human NSCLC cells, and suppress the tube formation in EA.hy926 cells. In addition, we used Lewis NSCLC xenograft model with 2 times to choose the suitable dosage of $C_3C_{12}PPD$ for vivo experiments before this study, and found that 10.0 mg/kg $C_3C_{12}PPD$ had better inhibitory activity than 2.5 mg/kg, 5.0 mg/kg and 20.0 mg/kg $C_3C_{12}PPD$. Furthermore, 10.0 mg/kg $C_3C_{12}PPD$ also significantly inhibited the tumor growth in A549 human NSCLC xenograft model.

The unlimited cell proliferation, angiogenesis and migration are associated with mortality of NSCLC. Raf/MEK/ERK signaling pathway plays an important role in tumorigenesis and progression.[26,27] In the present study, $C_3C_{12}PPD$ significantly inhibited the p-c-Raf, p-MEK and p-ERK in NSCLC cells and tumor tissues, suggesting that $C_3C_{12}PPD$ inhibited tumor growth of NSCLC partly through inhibiting the activity of Raf/MEK/ERK pathway. The AKT/mTOR and AKT/GSK-3β/β-Catenin signaling pathways have been confirmed to be associated

with cancer cell proliferation, metastasis and angiogenesis.[20,28,29] The inhibition of p-c-Raf also lead to the inhibition of p-AKT, then reduced the level of downstream proteins, p-mTOR, HIF-1α and VEGF, which are associated with migration and angiogenesis.[24] In addition, the inhibition of p-AKT also decreased the level of p-GSK-3β, β-Catenin, as well as its downstream proteins c-MYC, MMP2, which are confirmed to be involved in cell migration.[30–32] The results showed us that $C_3C_{12}PPD$ suppressed tumor growth, angiogenesis and migration in NSCLC by inhibiting of Raf/MEK/ERK, AKT/mTOR and AKT/GSK-3β/β-Catenin signaling pathways.[33–37] Furthermore, The IHC results also confirmed that tumor proliferation and angiogenesis were weakened following treatment with $C_3C_{12}PPD$ in Lewis xenograft tumors.

Furthermore, $C_3C_{12}PPD$ had little systemic toxicity at dose of 10.0 mg/kg in Lewis and A549 xenograft models, without decreasing the body weight of mice, or altering the hematological index, which are important indexes for the initial evaluation of drug safety.[38,39] Taken together, these results suggest that $C_3C_{12}PPD$ may serve as a potent candidate compound for the treatment of NSCLC.

This is the first study to report $C_3C_{12}PPD$ exhibit anti-non small cell lung cancer activity by inhibiting Raf/MEK/ERK, AKT/mTOR and AKT/GSK-3β/β-Catenin signaling pathways. Our work has laid a foundation for the research of $C_3C_{12}PPD$. However, there are still much work we need to do for the drug development of $C_3C_{12}PPD$, including the specific target on its anti-lung cancer activity, the toxicity, the pharmacokinetic characteristics and so on. We hope the study could make an experimental basis for its further study.

Conclusion

C_3C_{12}PPD showed inhibitory effect on proliferation, migration and angiogenesis of NSCLC, and may serve as a potential therapeutic candidate compound against NSCLC.

Ethics approval and informed consent

All animal studies were in compliance with policies of the Institute of Material Medical Animal Care and Use Committee. All animal protocols conformed to the Guidelines for the Care and Use of Laboratory Animals, and the study protocol was approved by the Animal Care and Use Committee of Chinese Academy of Medical Sciences and Peking Union Medical College.

Data availability

All data are fully available without restriction.

Abbreviations

C_3C_{12}PPD, 3-O-β-D-glucopyranosyl-12-O-β-D-glucopyranosyl-dammar-24-ene-3β, 12β, 20S-triol; NSCLC, non-small cell lung cancer; MTT, thiazolyl blue tetrazolium bromide; VEGF, vascular endothelial growth factor; DMEM, Dulbecco's modified Eagle's medium; FBS, fetal bovine serum; DMSO, dimethyl sulfoxide; p.o., gavage; H&E, hematoxylin and eosin.

Acknowledgment

Author contributions

All authors contributed to data analysis, drafting and revising the article, gave final approval of the version to be published, and agree to be accountable for all aspects of the work.

Disclosure

The authors report no conflicts of interest in this work.

References

1. Wang C, Kulkarni P, Salgia R. Combined checkpoint inhibition and chemotherapy: new era of 1(st)-line treatment for non-small-cell lung cancer. *Mol Ther Oncolytics*. 2019;13:1–6. doi:10.1016/j.omto.2019.02.001

2. Bray F, Ferlay J, Soerjomataram I, Siegel RL, Torre LA, Jemal A. Global cancer statistics 2018: GLOBOCAN estimates of incidence and mortality worldwide for 36 cancers in 185 countries. *CA Cancer J Clin*. 2018. doi:10.3322/caac.21492

3. Li H, Huang N, Zhu W, et al. Modulation the crosstalk between tumor-associated macrophages and non-small cell lung cancer to inhibit tumor migration and invasion by ginsenoside Rh2. *BMC Cancer*. 2018;18(1):579. doi:10.1186/s12885-018-4242-8

4. Mancuso C, Santangelo R. Panax ginseng and Panax quinquefolius: From pharmacology to toxicology. *Food Chem Toxicol*. 2017;107(Pt A):362–372. doi:10.1016/j.fct.2017.07.019

5. Patel S, Rauf A. Adaptogenic herb ginseng (Panax) as medical food: Status quo and future prospects. *Biomed Pharmacother*. 2017;85:120–127. doi:10.1016/j.biopha.2016.11.112

6. Xu W, Choi HK, Huang L. State of panax ginseng research: a global analysis. *Molecules*. 2017;22(9). doi:10.3390/molecules22091518

7. Ahuja A, Kim JH, Kim JH, Yi YS, Cho JY. Functional role of ginseng-derived compounds in cancer. *J Ginseng Res*. 2018;42 (3):248–254. doi:10.1016/j.jgr.2017.04.009

8. Lee SY, Kim GT, Roh SH, et al. Proteomic analysis of the anti-cancer effect of 20S-ginsenoside Rg3 in human colon cancer cell lines. *Biosci Biotechnol Biochem*. 2009;73(4):811–816. doi:10.1271/bbb.80 637

9. Sun M, Ye Y, Xiao L, Duan X, Zhang Y, Zhang H. Anticancer effects of ginsenoside Rg3 (Review). *Int J Mol Med*. 2017;39(3):507–518. doi:10.3892/ijmm.2017.2857

10. Liang H, Hu Z, Zhang T, et al. Production of a bioactive unnatural ginsenoside by metabolically engineered yeasts based on a new UDP-glycosyltransferase from bacillus subtilis. *Metab Eng*. 2017;44:60–69. doi:10.1016/j.ymben.2017.07.008

11. Dai L, Liu C, Li J, et al. One-Pot synthesis of ginsenoside Rh2 and bioactive unnatural ginsenoside by coupling promiscuous glycosyltransferase from bacillus subtilis 168 to sucrose synthase. *J Agric Food Chem*. 2018;66(11):2830–2837. doi:10.1021/acs.jafc.8b00597

12. Atopkina LN, Malinovskaya GV, Elyakov GB, et al. Cytotoxicity of natural ginseng glycosides and semisynthetic analogues. *Planta Med*. 1999;65(1):30–34.

13. He BC, Gao JL, Luo X, et al. Ginsenoside Rg3 inhibits colorectal tumor growth through the down-regulation of Wnt/ss-catenin signaling. *Int J Oncol*. 2011;38(2):437–445. doi:10.3892/ijo.2010.858

14. Hsieh YH, Deng JS, Chang YS, Huang GJ. Ginsenoside Rh2 ameliorates lipopolysaccharide-induced acute lung injury by regulating the TLR4/PI3K/Akt/mTOR, Raf-1/MEK/ERK, and Keap1/Nrf2/HO-1 signaling pathways in mice. *Nutrients*. 2018;10(9).

15. Yang J, Yuan D, Xing T, et al. Ginsenoside Rh2 inhibiting HCT116 colon cancer cell proliferation through blocking PDZ-binding kinase/T-LAK cell-originated protein kinase. *J Ginseng Res*. 2016;40 (4):400–408. doi:10.1016/j.jgr.2016.03.007

16. Mukhopadhyay T, Roth JA. Induction of apoptosis in human lung cancer cells after wild-type p53 activation by methoxyestradiol. *Oncogene*. 1997;14(3):379–384. doi:10.1038/sj.onc.1200835

17. Wu CT, Lin TY, Hsu HY, Sheu F, Ho CM, Chen EI. Ling Zhi-8 mediates p53-dependent growth arrest of lung cancer cells proliferation via the ribosomal protein S7-MDM2-p53 pathway. *Carcinogenesis*. 2011;32(12):1890–1896. doi:10.1093/carcin/bgr221

18. Li Y, Tang K, Zhang L, et al. The molecular mechanisms of a novel multi-kinase inhibitor ZLJ33 in suppressing pancreatic cancer growth. *Cancer Lett*. 2015;356(2 Pt B):392–403. doi:10.1016/j.canlet.2014.09.040

19. Mao G, Liu Y, Fang X, et al. Tumor-derived microRNA-494 promotes angiogenesis in non-small cell lung cancer. *Angiogenesis*. 2015;18(3):373–382. doi:10.1007/s10456-015-9474-5

20. Keremu A, Maimaiti X, Aimaiti A, et al. NRSN2 promotes osteosarcoma cell proliferation and growth through PI3K/Akt/MTOR and Wnt/beta-catenin signaling. *Am J Cancer Res*. 2017;7(3):565–573.

21. Liu L, Zhou XM, Yang FF, et al. TRIM22 confers poor prognosis and promotes epithelial-mesenchymal transition through regulation of AKT/GSK3beta/beta-catenin signaling in non-small cell lung cancer. *Oncotarget*. 2017;8(37):62069–62080. doi:10.18632/oncotarget.18 911

22. Wang S, Long S, Xiao S, Wu W, Hann SS. Decoction of Chinese herbal medicine fuzheng kang-ai induces lung cancer cell apoptosis via STAT3/Bcl-2/Caspase-3 pathway. *Evid Based Complement Alternat Med*. 2018;2018:8567905. doi:10.1155/2018/9567061

23. Yang J, Li S, Wang L, et al. Ginsenoside Rg3 attenuates lipopolysaccharide-induced acute lung injury via MerTK-dependent activation of the PI3K/AKT/mTOR pathway. *Front Pharmacol*. 2018;9:850. doi:10.3389/fphar.2018.00850

24. Zeng D, Wang J, Kong P, Chang C, Li J, Li J. Ginsenoside Rg3 inhibits HIF-1alpha and VEGF expression in patient with acute leukemia via inhibiting the activation of PI3K/Akt and ERK1/2 pathways. *Int J Clin Exp Pathol*. 2014;7(5):2172–2178.

25. Huang D, Ding Y, WM L, et al. Inhibition of MAPK kinase signaling pathways suppressed renal cell carcinoma growth and angiogenesis in vivo. *Cancer Res*. 2008;68(1):81–88. doi:10.1158/0008-5472.CAN-07-5311

26. Fang CY, Wu CZ, Chen PN, et al. Antimetastatic potentials of salvianolic acid A on oral squamous cell carcinoma by targeting MMP-2 and the c-Raf/MEK/ERK pathway. *Environ Toxicol*. 2018;33(5):545–554. doi:10.1002/tox.22542

27. Wang Y, Lin X, Fu X, et al. Long non-coding RNA BANCR regulates cancer stem cell markers in papillary thyroid cancer via the RAF/MEK/ERK signaling pathway. *Oncol Rep*. 2018;40(2):859–866. doi:10.3892/or.2018.6502

28. Vora SR, Juric D, Kim N, et al. CDK 4/6 inhibitors sensitize PIK3CA mutant breast cancer to PI3K inhibitors. *Cancer Cell*. 2014;26(1):136–149. doi:10.1016/j.ccr.2014.05.020

29. Jackson AL, Zhou B, Kim WY. HIF, hypoxia and the role of angiogenesis in non-small cell lung cancer. *Expert Opin Ther Targets*. 2010;14(10):1047–1057. doi:10.1517/14728222.2010.511617

30. Xu X, Li J, Sun X, et al. Tumor suppressor NDRG2 inhibits glycolysis and glutaminolysis in colorectal cancer cells by repressing c-Myc expression. *Oncotarget*. 2015;6(28):26161–26176. doi:10.18632/oncotarget.4544

31. Yang W, Lu Z. Regulation and function of pyruvate kinase M2 in cancer. *Cancer Lett*. 2013;339(2):153–158. doi:10.1016/j.canlet.2013.06.008

32. Yang Z, Li K, Liang Q, et al. Elevated hydrostatic pressure promotes ameloblastoma cell invasion through upregulation of MMP-2 and MMP-9 expression via Wnt/beta-catenin signalling. *J Oral Pathol Med*. 2018;47(9):836–846. doi:10.1111/jop.12761

33. Polivka J Jr., Janku F. Molecular targets for cancer therapy in the PI3K/AKT/mTOR pathway. *Pharmacol Ther*. 2014;142(2):164–175. doi:10.1016/j.pharmthera.2013.12.004

34. Wu A, Li M, Mai Z, Li S, Yang Z. [CK2alpha regulates the metastases and migration of lung adenocarcinoma A549 cell line through PI3K/Akt/GSK-3beta signal pathway]. *Zhongguo Fei Ai Za Zhi*. 2017;20(4):233–238. doi:10.3779/j.issn.1009-3419.2017.04.11

35. Wu GJ, Pen J, Huang Y, et al. KAP1 inhibits the Raf-MEK-ERK pathway to promote tumorigenesis in A549 lung cancer cells. *Mol Carcinog*. 2018;57(10):1396–1407. doi:10.1002/mc.22853

36. Zhang X, Jiang G, Sun M, et al. Cytosolic THUMPD1 promotes breast cancer cells invasion and metastasis via the AKT-GSK3-Snail pathway. *Oncotarget*. 2017;8(8):13357–13366. doi:10.18632/oncotarget.14528

37. Iwadate Y. Epithelial-mesenchymal transition in glioblastoma progression. *Oncol Lett*. 2016;11(3):1615–1620. doi:10.3892/ol.2016.4113

38. Yang J, Li L, Xu C, Yang D, Wang S, Yuan S. CT1042, a novel anticancer agent, exhibits effects by activating p53 and inhibiting survivin. *Oncol Rep*. 2018;39(6):2759–2768. doi:10.3892/or.2018.6354

39. Zhang C, Wang W, Liu T, et al. Doxorubicin-loaded glycyrrhetinic acid-modified alginate nanoparticles for liver tumor chemotherapy. *Biomaterials*. 2012;33(7):2187–2196. doi:10.1016/j.biomaterials.2011.11.045